Effects of Biofilms and Particle Physical Properties on the Rising and Settling Velocities of Microplastic Fibers and Sheets

Isabel Jalón-Rojas, Alicia Romero-Ramírez, Kelly Fauquembergue, Linda Rossignol, Jérôme Cachot, Damien Sous, Bénédicte Morin

Effects of biofilm and particle physical properties on the rising and settling velocities of microplastic fibers and sheets

Isabel Jalón-Rojas[1,*], Alicia Romero-Ramírez[2], Kelly Fauquembergue[3], Linda Rossignol[4], Jérôme Cachot[5], Damien Sous[6,7], Bénédicte Morin[8]

[1] UMR5805 EPOC, CNRS, Univ. Bordeaux, 33615, Pessac, France

[2] UMR5805 EPOC, CNRS, Univ. Bordeaux, 33615, Pessac, France

[3] UMR5805 EPOC, CNRS, Univ. Bordeaux, 33615, Pessac, France

[4] UMR5805 EPOC, CNRS, Univ. Bordeaux, 33615, Pessac, France

[5] UMR5805 EPOC, CNRS, Univ. Bordeaux, 33615, Pessac, France

[6] Univ Pau & Pays Adour/E2S UPPA, Laboratoire des Sciences de l'Ingénieur Appliquées à la Méchanique et au Génie Electrique - Fédération IPRA, EA4581, 64600, Anglet, France

[7] Université de Toulon, Aix Marseille Université, CNRS, IRD, Mediterranean Institute of Oceanography (MIO), 83130, La Garde, France

[8] UMR5805 EPOC, CNRS, Univ. Bordeaux, 33615, Pessac, France

* Correspondence to: Isabel Jalón-Rojas (isabel.jalon-rojas@u-bordeaux.fr)

ABSTRACT

Vertical dynamics of microplastics (MPs) in the water column are complex and not fully understood due to the diversity of environmental MPs and the impact of weathering and biofouling on their dynamical properties. In this study, we investigate the effects of the particle properties and biofilm on the vertical (settling or rising) velocity of microplastic sheets and fibers under laboratory conditions. The experiments focus on 3 types of MPs (polyester PES fibers, polyethylene terephthalate PET sheets, and polypropylene PP sheets) of 9 sizes and 2 degrees of biological colonization. Even though pristine PES fibers and PET sheets had a similar density, the sinking velocity of fibers was much smaller and independent of their length. The settling or rising velocity of sheets increased with the particle size up to a threshold and then decreased due to the wake of horizontal oscillations in large particles. Biofilm had unexpected effects on vertical velocities. Irregular biofilm distributions can trigger motion instabilities that decrease settling velocities of sheets despite the increase of density. Biofilm can also modify the orientation of fibers, which may increase their settling velocity. Finally, we selected the most performant theoretical formulation for each type of particle and proposed modifications to consider the effect of biofilm distribution.

KEYWORDS: microplastics, vertical velocity, biofilm, physical properties, transport.

SYNOPSIS: There is a lack of knowledge of the effects of biofilm on microplastic dynamics. This study reports the modifications in the (rising or settling) terminal velocity of microplastics due to biofilm, with implications for microplatic transport in the aquatic environment.

GRAPHIC FOR TABLE OF CONTENTS

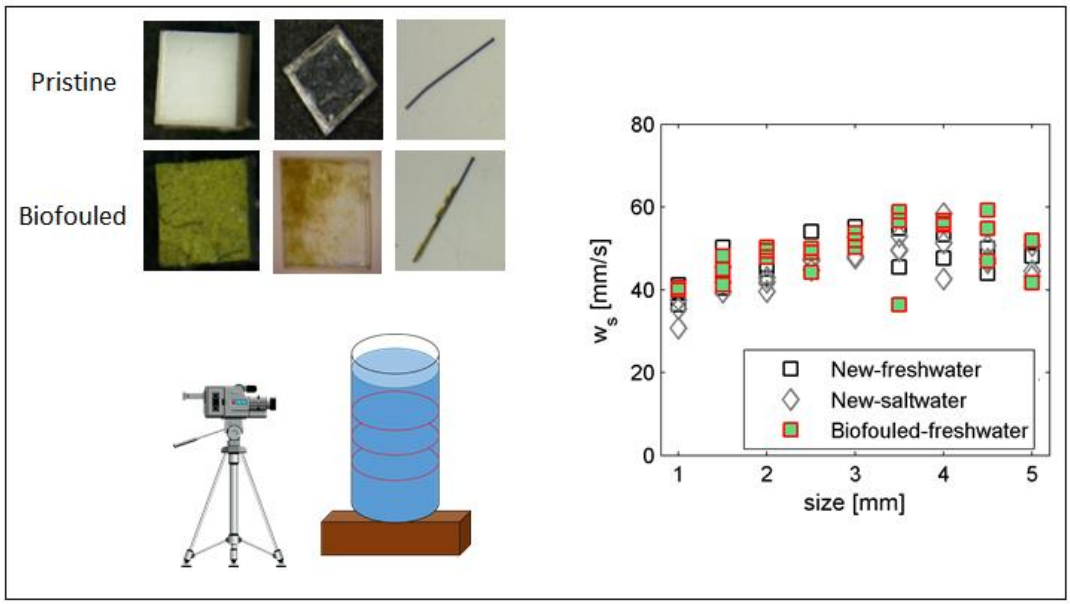

Introduction

Plastics are accumulating in the aquatic environment due to the increased production and their low biodegradability rate. In particular, microplastic (MP) particles and fibers (<5 mm in size) are considered emergent pollutants of great concern due to their persistence and ability to be transported over large distances, leading to adverse effects to aquatic ecosystems and human well-being[1–4]. Consequently, an intensified research effort is being devoted to understanding the amount of MPs found at different aquatic environments and compartments[5–8] and the mechanism driving their presence, transport, and persistence[9–11].

MP dynamics and transport processes in aquatic systems are complex. Besides environmental forcings and hydrodynamic processes, the transport of MPs depends on their dynamical properties, in particular on the vertical (settling or rising) velocity[12–14]. Recent modeling studies have demonstrated that, likewise sediments, the trajectories of MPs and the influence of physical processes driving them are very sensitive to this velocity[15–18]. The settling, terminal, or sinking velocity is the rate at which a negatively buoyant particle settles through a still fluid[19,20]. The rising or upward terminal velocity is the analogous parameter for positively buoyant particles[12]. Both parameters reflect the balance between gravitational, buoyancy and drag forces, and depend on the particle physical properties (density, size, shape, roundness, surface texture) [20–24].

MPs exhibit diverse physical properties (e.g. density range from <0.05 g/cm^3 to 2.3 g/cm^3) and, consequently, a wide range of vertical velocities. Recent experimental studies have measured the vertical velocity of pristine MPs of different densities, sizes, and shapes under laboratory conditions, and tested or proposed different drag model to describe this parameter quantitatively[23–26]. All these studies highlighted the effects of the particle density, size, and shape on the vertical velocity. While Khatmullina and Isachenko[24] and Waldschläger and

Schüttrumpf[25] put forward different drag models for particles of different shapes (i.e. spheres, fragments, fibers), Melkebeke et al.[26] proposed a single formulation for all the types of MPs. However, these studies did not cover the entire spectrum of MPs present in the environment. More measurements are therefore necessary, in particular to describe the vertical transport of small fibers and thick sheets, which are commonly detected in the aquatic environment[27]. And most importantly, previous studies mainly focused on pristine particles not affected by biota or environmental conditions.

When MPs reach the environment, they are affected by weathering, biofouling, aggregation, abiotic and biotic degradation, and other external factors[28–31]. Consequently, their physical and dynamical properties vary with the time spent in the environment. Biofouling has been identified as one of the processes that most affect particle density and its sinking capacity[16,32–35]. The colonization of MPs surface by microorganisms is supposed to be particularly important to transform negatively buoyant particles into positively buoyant and make them sink below the water surface[35,36]. However, experimental studies quantifying the effects of biofouling on vertical velocity are rare. Kaiser et al.[22] incubated spherical 1 mm size MPs of polystyrene and polyethylene in estuarine and coastal waters under laboratory conditions and determined that biofouling significantly changed their sinking behavior after 6 weeks of incubation. Karkanorachki et al.[37] established empirical relationships between biofilm growing and sinking velocity for 3 pellets and 5 films. Further research is therefore needed to understand how the combination of different properties (size, shape, density change by biofilm) affect the vertical velocity of MPs exposed to *in situ* environmental conditions.

The present study aims to understand and quantify the effects of the particle properties and biofilm on the settling and rising velocities of MPs, and evaluate the relevance of theoretical drag models to predict these parameters. To this end, we conducted seven sets of laboratory

experiments to determine the vertical velocity of pristine and biofouled fibers and sheets of different polymer types and sizes, using both fresh and saltwater.

Materials and Methods

Selection and generation of particles. The experiments focus on three types of particles - polypropylene (PP) sheets, polyethylene terephthalate (PET) sheets, and polyester (PES) fibers – with two degrees of biofilm colonization and aging – pristine and aged during 3 months in the ocean (Fig 1.a). These particles were selected based on their wide spreading in the aquatic environment[38,39], aiming at completing precedent experimental studies that lack small fibers and sheet particles. PP and PET are two of the most highly produced and commonly used non-fiber plastics in the world[40]. These polymers are characterized by a high ratio between production and waste[25] as they are mostly used for plastic packages and bottles that break down into small sheet fragments due to weathering and fragmentation processes. PES fibers are the most produced synthetic fibers[40], commonly used in clothing and fishing nets. The particles used in this experiment were thus produced from a water bottle (PET), a white bucket (PP), and a boat rope (PES). The polymer type was characterized using a Fourier-Transformed Infrared spectrometer (FTIR) with an attenuated Total Reflectance (ATR) diamond crystal attachment (Thermo Nicolet Nexus 870) equipped with an MCT detector. All spectra were recorded with the OMNIC software (V9.2.98) at a resolution of 4 cm^{-1}. The ATR-FTIR spectra were compared to different libraries provided by Thermo Fisher (HR Hummel Polymer and additives and HR Specta Polymers and Plasticizers by ATR).

For plastic aging, materials were cut into pieces 5x5 cm with scissors. 8 replicates of each material were directly stored at 4ºC until the production of pristine MPs. Other 8 replicates were

placed and fixed in oyster bags and exposed to *in situ* environmental condition in Arcachon Bay (SW France) from 10 November 2019. They were attached to a navigational beacon (44°41'18.5"N 1°09'34.6"W) and immersed at a water depth varying from 1 to 4 m, depending on the tide. The samples were recovered after 3 months and stored at 4º C until the production of aged, biofouled plastics. Pristine and biofouled PP sheets, PET sheets, and PES fibers of 9 sizes were then produced from the stored samples with a scalpel under a binocular stereoscope (Kern, OZO 553). All sheets had a regular quadrilateral shape (Fig 1.a) to facilitate evaluating the effect of size. Sizes (fiber length and sheet side) ranged from 1 to 5 mm with a step of 0.5 mm and a maximum error of ± 0.1 mm. We produced 3 replicates for each size, which rendered a total of 162 particles. ODC825 microscope camera and Microscope VIS software were used to measure the three dimensions of each particle and to generate high-resolution 2D images (see examples in Fig. 1.a). PP and PE thickness were 1.5 and 0.3 mm, respectively; fibers diameter was 30 μm.

Two additional plastic particles were used to validate the experiments: polystyrene (PS) spheres perfectly round with a certified density of 1.05 g/cm^3 and certified mean diameters of 4.7 mm (± 0.1 mm) and 1.94 mm (± 0.05 mm). We also considered 3 replicates of each type of particle.

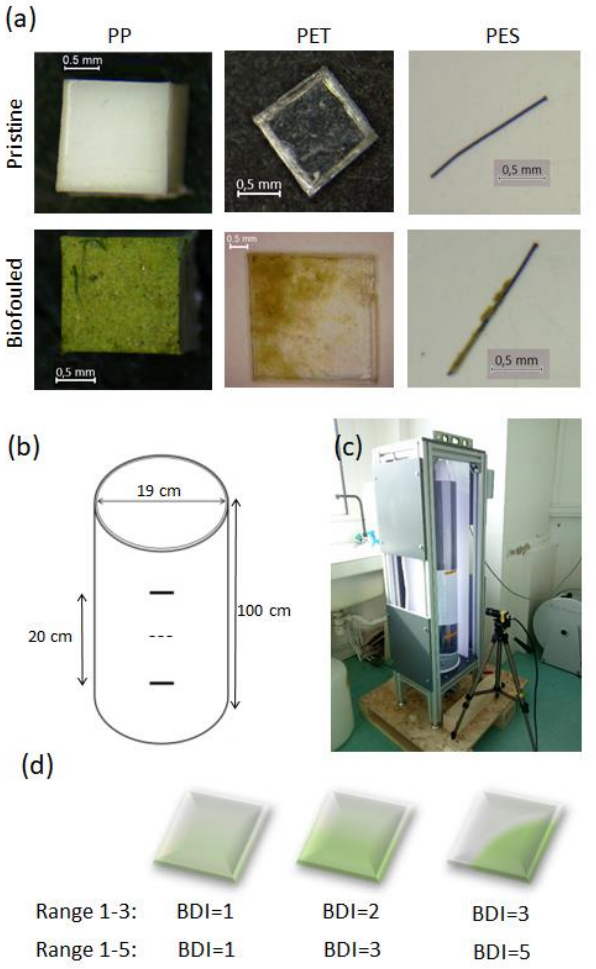

131

132 **Figure 1**. (a) Digital photographs of the type of MPs used in the experiments: pristine and biofouled Polypropylene (PP)
133 sheets, polyethylene terephthalate (PET) sheets, and polyester (PES) fibers; (b) Column dimensions; (c) Photograph of the
134 experimental setup; (d) Chart to quantitatively estimate the distribution of biofilm thought the biofilm distribution index
135 (BDI).

136 **Size, shape and biofilm distribution characterization.** Particle size was characterized by four
137 parameters largely used in studies on sediment and microplastic behavior[20,25,41]: (1) the particle
138 length L [m] (fiber length or sheet side), (2) the particle thickness THK [m] (fiber diameter or
139 sheet thickness), (3) the equivalent particle diameter d_{equi} [m] (Eq 1), and (4) the dimensionless
140 diameter D* [-] (Eq 2):

141 $$d_{equi} = \sqrt{abc} \quad \text{(Eq. 1)}$$

142 $$D * \left(\frac{\Delta g}{\nu^2}\right)^{1/3} d_{equi} \quad \text{(Eq. 2)}$$

where a, b, c are the longest, intermediate, and shortest sides [m], g is the gravity acceleration [9.8 m/s^2], ν is the kinematic viscosity of the fluid [10^{-6} and 1.04_x10^{-6} m^2/s for fresh and saltwater, respectively[42]], and Δ describes the ratio of particle density ρ_s [kg/m^3] to water density ρ_w [kg/m^3]:

$$\Delta = \left|\frac{\rho_s - \rho_w}{\rho_w}\right| \quad \text{(Eq. 3)}$$

The shape was quantified through four parameters typically used in drag models (Section 2.5): the Power roundness P, the Corey shape factor CSF, sphericity Φ, and circularity χ. P is determined by two independent observers (mean value) and ranges from 1 (angular particles) to 6 (well-rounded particles)[43]. CSF is calculated from the three mean side lengths of the particle (a, b, and c already defined in Eq 1) as shown in Eq 4.

$$CSF = \frac{c}{\sqrt{ab}} \quad \text{(Eq. 4)}$$

Sphericity Φ is defined as the ratio of the surface area of the equivalent sphere and the particle surface area. It quantifies the difference of particle shape from a perfect sphere (for which Φ = 1, see Dioguardi et al.[44] for more details). Circularity χ is defined as the ratio between the maximum projection perimeter and the perimeter of the circle equivalent to the maximum projection area of a particle (see Dioguardi et al.[44] for details). It is greater than 1, being 1 for a perfect circular contour. Table 1 summarizes the main characteristics of the particles.

PP sheets presented a homogeneous cover of biofilm while PET sheets presented biofilm patches (see examples in Fig. 1.a) whose distribution (more or less irregular) varied among the different particles. In order to quantify these differences in biofilm distribution, we defined a Biofilm Distribution Index (BDI) and tested two ranges of values: from 1 for well-distributed biofilm, to 3 or 5 for irregular-distributed biofilm (Fig. 1.d). The assigned value is the average of values attributed by two independent observers, analogously to the Power

roundness used to characterized MP shape[25]. As PET sheets were transparent, the biofilm distribution of both sides was considered simultaneously for the BDI definition. In the case of no transparent particles, BDI can be calculated as the mean value of both sides.

Table 1. Properties of MPs selected for the experiments.

Polymer and shape	Size/ Length L [mm]	dequi [mm]	Exposure time [months]	Density (estimated) [g/cm3]	P	CSF	Φ	X
PP sheets	1-5 (± 0.1)	1-3.35	0	0.890 (±0.006)	4	1(1mm) – 0.3 (5mm)	0.79 (1mm)- 0.68 (5mm)	1.13
			3	0.892- 0.918 (±0.004)	4	1(1mm) – 0.3 (5mm)	0.79 (1mm)- 0.68 (5mm)	1.13
PET sheets	1-5 (± 0.1)	0.67-1.96	0	1.220 (±0.014)	4	0.30 (1 mm)- 0.06 (5mm)	0.67 (1mm) – 0.33 (5mm)	1.13
			3	1.180-1.350 (±0.020)	4	0.30 (1 mm)- 0.06 (5mm)	0.67 (1mm) – 0.33 (5mm)	1.13
PES fibers	1-5 (± 0.1)	0.10-0.17	0	1.17 (±0.03)	1	0.17 (1 mm)- 0.08 (5mm)	0.40 (1mm) – 0.24 (5 mm)	3.35 (1mm) – 7.33 (5mm)
			3	1.14-1.60 (±0.01)	1	0.17 (1 mm)- 0.08 (5mm)	0.40 (1mm) – 0.24 (5 mm)	3.35 (1mm) – 7.33 (5mm)

Density determination. Particles density was estimated using a variation of the titration method according to DIN 53 479 and previous experimental studies[24,25]. PET and PES particles, denser than water, were placed in a 50 ml test tube of distilled water and agitated to release all possible air bubbles. When the particle sank to the bottom, the initial distilled water solution was progressively densified by the dropwise addition of concentrated zinc chloride solution (ρ=1700 kg/m^3) using a burette. The procedure continued until the solution reached the density of the particle, and the particle rose and floated in the liquid for 1 minute without rising or falling. In the case of PP particles, less dense than water, the density determining liquid was

ethanol (95%; ρ=789 kg/m^3). For each particle, a volume of 1 mL of solution was collected with an automatic pipet and weighed using a high precision electronic balance to determine its density and therefore the density of the particle. This last step was repeated 5 times in order to estimate the error associated with this method (Table 1). The density of pristine particles was estimated as the average density of 3 particles randomly selected for each type of polymer. Density was in turn estimated for each individual biofouled particle. The range of estimated densities (mean and standard deviation) is summarized in Table 1.

Experimental setup. The experimental setup was inspired by the one used in Waldschläger and Schüttrumpf[25] to measure both rising and settling velocities. It consists of a transparent polycarbonate cylindrical column, 1m high and 19 cm in internal diameter, located in a steady room temperature (20°C, Fig. 1b-c). The internal diameter, similar to that used in previous studies[24,25], is large enough to neglect wall effects[45]. For experiments dedicated to rising velocities, MPs are inserted at the base of the column through an ad-hoc gate at the center of the column. Once the gate is closed, the particle rises throughout the column to be finally recovered at the free surface. For experiments dedicated to settling velocity, particles were placed in the center of the column approximately 1 cm below the water surface to avoid their retention by surface tension. Lateral illumination is provided by white LED bands stuck on the column lateral sides. Water temperature was monitored using a mercury thermometer. Temperature variation during each experiment was lower than 0.5ºC.

Six sets of experiments (3 types of particles x 2 colonization degrees) were performed using distilled freshwater (ρ=0.998 g/cm^3) to exclude the influence of other water components (minerals, suspended solids), similarly to previous studies[23–26]. An extra set was performed for all the pristine PET sheets using saltwater (ρ=1.026 g/cm^3) from La Salie Beach (French Atlantic coast) in order to compare results and evaluate the pertinence of theoretical models using waters with different densities. The validation experiments with certified spherical

particles were also performed with both fresh- and saltwater. Particles were placed in the same liquid as inside the column before the experiment. To minimize the potential loss of biofilm, we chained the particle generation, density measurements, and vertical velocity experiments over three consecutive days for each type of particle.

Image acquisition and analysis. The rising and settling velocities of the different particles were calculated by measuring the time that a particle employs to move over a known distance of 20 cm in a vertical column. The location of the measurement area was placed at least 15 cm away from the top and bottom of the water column to give the particle the possibility to reach the terminal velocity[24,25]. The 20 cm vertical distance was divided into two sections of 10 cm so that time that a particle need to cross these two sections as measured and compared to ensure that there was no further acceleration. Time was precisely measured by recording a time-lapse series of images with a uEye U3-3890CP-M-GL camera. The frequency of acquisition was settled to 0.1 Hz for fibers and 0.05 Hz for sheets.

We performed statistical analysis to compare the results from the different experimental sets. We used parametric tests (T-Test or ANOVA) when data or their transforms (like a log or cubic root) met the normality and homoscedasticity, and non-parametric tests (Mann-Whitney U test or Kruskal-Wallis) otherwise. We refer to data sets as "significantly different" when these tests were statistically significant at $p < 0.05$.

Evaluation of drag models. We evaluated the performance of different theoretical drag models to estimate the observed vertical velocities of pristine and biofouled fibers and sheets by comparing observations and predictions through the relative error E (%) and the root mean square error RMSE (mm/s). Previous experimental studies[24–26] already evaluated the prediction capacity of numerous empirical formulations, particularly for pristine MPs settling velocities, and some of them proposed new formulations. In this study, we built on previous works and

evaluated the formulations that previously showed the best fit according to these works. For settling velocities, we selected Waldschläger's formulation[25], Diouardi's formulation[44], Dellino's formulation[46], Zhiyao formulation[47] and Khatmullina's formulation for fibers[24] (see formulations in Table 2). To our knowledge, only Waldschläger's formulation has been proposed for rising velocities so far, but we also tested formulations proposed for settling velocity. Most of these formulations consist of estimations of the dimensionless drag coefficient C_D, which quantifies the drag force and depends on the particle density, shape, size, and/or Reynolds number:

$$\Re_P = \frac{\rho_w w_v d_p}{\mu} \quad \text{(Eq. 5)}$$

where d_p is the particle size (d_{equi}, L, or THK depending on the formulation) [m] and μ is the water dynamical viscosity [Pa/s]. The shape is considered through the different shape parameters (e.g. CSF, P, χ, Φ), depending on the model. The settling or rising velocity is calculated from the Stokes formula, which represents the balance between gravitational, buoyancy, and drag forms.

$$w_v = \sqrt{\frac{4}{3}\frac{d_p}{C_D}\Delta g} \quad \text{(Eq. 6)}$$

For C_D formulations dependent on Re, the vertical velocity is calculated iteratively until the assumed velocity for the Reynolds number corresponds to the calculated one.

Table 2. Drag models evaluated or proposed in this work.

Reference	Drag model	Size indicator
	RISING VELOCITY	
Waldschläger and Schüttrumpf (2019)	$C_{D,fibers} = \left(\frac{20}{\Re_p} + \frac{10}{\sqrt{\Re_p}} + \sqrt{1.195 - CSF}\right) \times \left(\frac{6}{P}\right)^{1-CSF}$	Sheets: L

	$C_{D,non-fibers} = \frac{3}{CSF \times \sqrt[3]{\Re_p}}$	
	SETTLING VELOCITY	
Waldschläger and Schüttrumpf (2019)	$C_{D,fibers} = \frac{4.7}{\sqrt{\Re_p}} + \sqrt{CSF};$ $C_{D,non-fibers} = \frac{3}{CSF \times \sqrt[3]{\Re_p}}$	Fibers: THK; Sheets: L
Dioguardi et al. (2018)	$C_D = \frac{24}{\sqrt{\Re_p}}\left(\frac{1-\Psi}{\Re_p}+1\right)^{0.25} + \frac{24}{\sqrt{\Re_p}}\Re_p{}^{0.6459}\Psi^{-\Re_p{}^{0.08}} + \frac{0.4251}{1+\frac{6880.95}{\Re_p}\Psi^{5.05}}$	Fibers: d_{equi} Sheets: L
Khatmullina and Isachenko (2017)	$w_s = \frac{\pi g \Delta}{2\nu}\frac{THK \times L}{55.238L + 12.691}$	-
Zhiyao et al. (2008)	$C_D = \left[\left(\frac{\sqrt{3}A}{2D_*^{3/2}}\right)^{2/n} + B^{1/n}\right]^n$ Zhiyao's coefficients : A=24, B=4/9, n=2	Fibers: d_{equi} Sheets: d_{equi}
Dellino et al. (2005)	$C_D = \frac{0.9297}{\Psi^{5.05}\Re_p{}^{0.0799}}$	Fibers: THK; Sheets: L
This work (Dellino'formulation including BDI)	$C_{D,sheets} = \frac{0.9297}{\Psi^{5.05}\Re_p{}^{0.0799}} BDI^{0.573}$	Sheets: L

Results and discussion

Validation. The settling velocity of certified PS spheres was determined in the upper and lower sections of the measurement area using fresh and saltwater. We first compared the velocities at the two sections to verify that no further acceleration acted on the particle, and found no significant differences (T-test, p=0.99; R^2=0.999). This provided a first validation of the position of the measurement area and allowed us to use the average value of the two sections

253 in the following evaluations. The velocities of the three runs (one run per replicate) were then
254 compared to check the reproducibility of the experiment (Fig. 2.a). We also checked that
255 measured velocities increased with the particle size and particle relative density as expected
256 (Fig. 2.a-b), and compared them with the velocities estimated with the different drag models.
257 A particular good estimation was obtained using the Waldshäger's formulation for spherical
258 MPs for both fresh and saltwater (E=5.2%, RMSE=4.5 mm/s, R^2=0.99). We concluded that our
259 experimental setup and measurement methodology was valid and repeatable and our results
260 were reliable. An extra comparison of the velocities in the upper and lower sections for all the
261 particles confirmed that there were no significant differences (T-test, p=0.70; R^2=0.991),
262 reinforcing this validation.

263 **Effect of physical properties.** Figure 2.c-h shows the settling (c-f) and rising (g-h) velocities
264 of the three types of particles as a function of their length and dimensionless diameter D*, a
265 parameter that takes into account size and density (Eq. 2). The sinking behavior of fibers and
266 sheets was completely different from each other, and different from the behavior of spherical
267 particles. Even though pristine PES fibers and PET sheets had a similar density (Table 2), the
268 sinking velocity of fibers was much smaller (Fig 2.b-c): all pristine fibers sank at a similar
269 velocity (2±0.45 mm/s in freshwater) regardless of their length (Fig 2.c). This behavior was
270 already observed in Waldschläger and Schüttrumpf[25] and is confirmed in the present study
271 through the systematic analysis of fibers with the same density and growing lengths. In fact, the
272 variability in measurements across the different lengths is comparable to the variability
273 observed between the three replicates of a given size (Fig 2.c). This variability may be
274 associated with little variances from the straight trajectories, which may rely on the fiber
275 orientation[48]. Nevertheless, most of the pristine fibers were aligned horizontally along their
276 vertical paths as previously observed by Khatmullina and Isachenko[49] and Waldschläger and

277 Schüttrumpf[25]. This is because the high- and low-pressure areas at the fiber ends hold the fiber
278 in the horizontal plane[50]

279 Pristine PET and PP sheets exhibited a similar behavior in their respective downward and
280 upward trajectories. PET sheets sank at velocities ranging from 36.4 to 59.3 mm/s in freshwater
281 (from 30.0 to 58.4 mm/s in saltwater, Fig 2. e-f) while PP sheets rose at velocities ranging from
282 35.4 to 74.0 mm/s in freshwater (Fig 2.g-h). In both cases, vertical velocity increased with the
283 particle size up to a threshold, 3.5-4 mm length, and then decreased. This behavior, observed in
284 both fresh and saltwater experiments, is related to the fact that larger sheets oscillated around a
285 horizontal axis in their own plane during their vertical trajectory, which slowed down their
286 vertical motion. This is consistent with the dynamics of falling of thin circular disks in still
287 water reported by Zhong et al.[51]. The disks performed a planar zigzag motion whose horizontal
288 oscillation increased with the Reynolds number (Eq. 5) up to a critical Reynolds number value.
289 Therefore, sheet size plays an important role in both sides of the force balance that determines
290 the vertical velocity: it increases the downward or upward force (gravity minus buoyancy), but
291 also enhance the Reynolds number (i.e. predominance of inertial forces over viscous forces)
292 and thus the drag force, which can wake instabilities and cause an unsteady motion of sheet
293 MP. This behavior has not been reported in previous studies on microplastics and differs from
294 the behavior of spherical pellets and (non-flattened) fragments whose settling and rising
295 velocity increases with length and dimensionless diameter[25,26,52]. These results reinforce thus
296 previous evidence on the key role of particle shape on the MP settling and rising behavior.
297 Regarding the effect of the fluid density, settling velocities of PET sheets were (significantly,
298 T-test, $p=0.018$) lower in saltwater than in freshwater as expected.

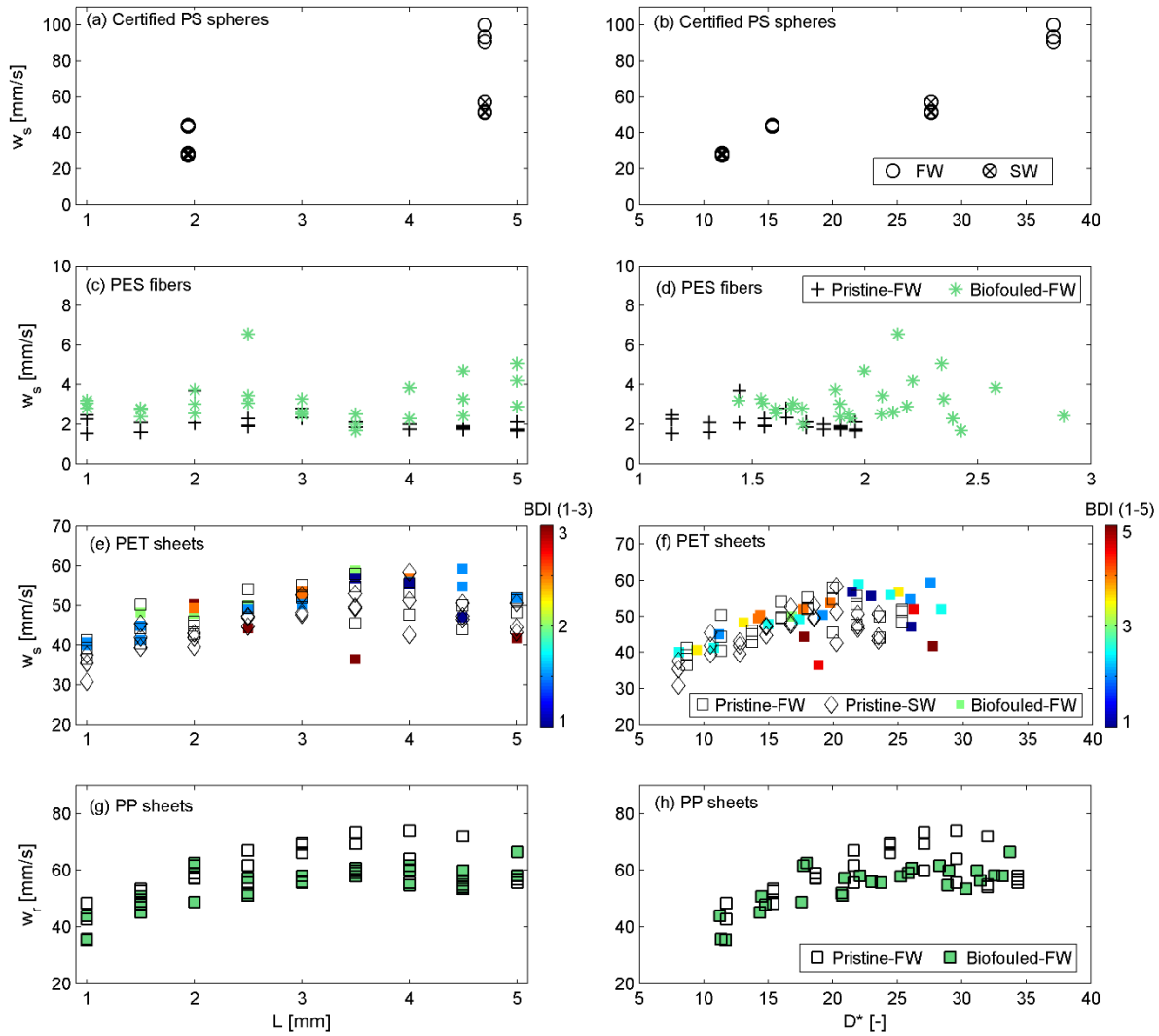

299

300 **Figure 2**. Settling (ws) and rising (wr) velocities of pristine and biofouled MPs as a function of the particle size (left column)
301 and the dimensionless diameter (right column): (a-b) certified spheres; (c-d) polyester (PES) fibers; (e-f) polyethylene
302 terephthalate (PET) sheets (0.3 mm thickness); (g-h) polypropylene (PP) sheets (1.5 mm thickness). FW and SW denotes
303 experiments performed in fresh- and saltwater, respectively. The color bars in (e) and (f) represent the biofilm distribution
304 index (BDI).

305

306 **Effect of biofilm.** We compared the vertical velocity of equivalent pristine and bioufouled MPs
307 and found different effects of biofilm depending on the type of particle (Fig 2. c-h). In the case
308 of PES fibers, settling velocities of biofouled particles (1.8-6.5 mm/s) were (significantly,
309 Mann-Whitney U test, $p<0.0001$) higher than pristine ones (1.7-3.7 mm/s). This may be related

to the increase of density by biofilm, from around 1.17 g/cm^3 up to 1.6 g/cm^3 (Table 1, Figure 2.d). However, the settling velocity did not show a clear dependency on density for this type of particle (Fig. 3). Part of this trend can be explained by the incertitude in determining densities. Another potential factor is that biofouled fibers presented different orientations during their fall. We identified fibers falling with clear vertical (or diagonal) orientations, which indeed had relatively higher settling velocities (Fig 3, Mann-Whitney U test, p=0.000). We explored if the orientation was related to a particular distribution pattern of biofilm but we could not derive a clear trend. Nevertheless, the order of magnitude of biofouled and pristine fiber velocities was relatively similar, especially taking into account that settling velocities of MPs present in the aquatic environment range from 1 to more than 100 mm/s[23,26].

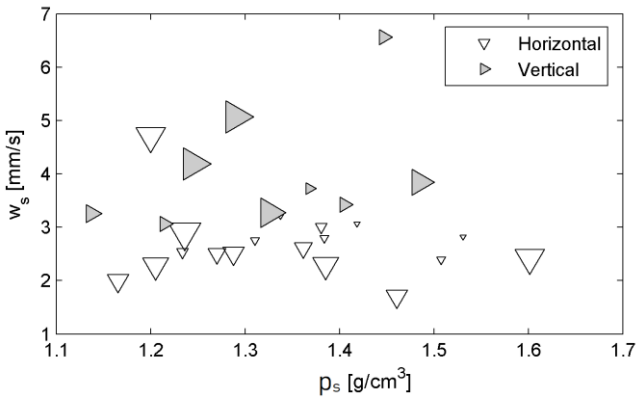

Figure 3. Vertical velocity of biofouled fibers as a function of the particle density. The (horizontal or vertical/inclined) alignment of fibers during their vertical motion is highlighted. Marker size represents the relative size of fibers.

The settling velocities of pristine and biofouled PET sheets showed no significant differences (T-Test, p=0.38) despite the overall increase in density after 3-month in aging (Table 1; higher D* for biofouled particles in Fig. 2.f). Surprisingly, some biofouled particles characterized by higher densities than their equivalent pristine particles had relatively lower settling velocities. Further insight was gained by analyzing the individual trajectories and biofilm distribution for

each of these peculiar cases. We observed that (1) they showed great horizontal oscillations over their vertical trajectories and (2) they were characterized by patches of abundant biofilm irregularly distributed over the particle surface (see biofouled PET sheet in Fig 1.a). To confirm and quantify this behavior we plotted sinking velocities of biofouled PET as a function of the Biofilm Distribution Index (BDI, Section 2) for two BDI ranges (from 1 for well distributed biofilm, to 3 or 5 for irregular distributed biofilm, Fig. 2.e and 2.f). We confirmed that particles characterized by high BDI had relatively smaller setting velocities. Similarly to size, biofilm can play a double role on the vertical velocity of sheets: it increases the gravity force but, depending on their distribution, it can cause unsteady motion of MPs and increase drag forces. Therefore, the vertical velocity of sheets relies on the nature, degree, and distribution of biofilm. The two tested ranges of BDI captured this behavior. To our knowledge, this is the first time that this behavior is reported in the literature.

Biofouled PP sheets had (significantly, T-test, $p=0.03$) lower raising velocities (35.4-62.5 m/s) than pristine ones (42.7-74 m/s) (Fig. 2.g-h). Unlike PET sheets, all biofouled PP sheets presented a thin cover of biofilm homogeneously distributed (Fig. 1.a) that had no impact on the particle oscillations. Therefore, biofilm only increased the particle density (Table 1), decreasing in turn the relative density (see lower D* for the same size in Fig. 2.h) and slowing down their raising motion.

Even if the analysis of biofilm growing is beyond the scope of this paper, we can highlight that a 3 months exposure period was not long enough for most PET sheets to exhibit a significant change in their settling velocity, and for PP sheets to exhibit negative buoyancy, even if a mature biofilm layer was developed. This supposes a relatively lower impact of biofilm on vertical velocities for similar exposure periods compared to other studies. Fazey and Ryan[53] found that low-density polyethylene (LDPE) and (high-density polyethylene (HDPE) films needed at least 66 days of exposition to start sinking. Kaiser et al.[22] showed that the settling

velocity of PS particles increased by 81% after 42 days in marine water. Amaral-Zettler et al.[35] demonstrated that HDPE and LDPE particles required around 6 weeks of immersion in the coastal waters of the North Sea to become negatively buoyant. The present study supports the results by Karkanorachaki et al.[37] that demonstrated that the nature and degree of biofouling, and consequently the variability rates of vertical velocity, vary for different polymers, shapes and environmental conditions. As in the present work, Karkanorachaki's experiments showed that their PP film samples were mainly covered by biofilm and less by macro-organisms, requiring relatively long periods to change vertical velocity significantly. The great thickness of PP sheets could also favor this behavior. It should also be noted that the required particles manipulation could carry a potential minor loss of biofilm. Still, we took great precautions and supervised that no significant loss occurred during both particles generation and density measurements.

Comparison with theoretical models. We evaluated the relevance of the selected drag models (Table 2, Section 2) to describe the vertical velocity of pristine and biofouled fibers and sheets. Table 3 compares the results of the physical experiments with the theoretical estimations, highlighting the equations providing the lowest relative (E) and root mean square (RMSE) errors. For each formulation and each type of particle, we tested different size indicators (L, d_{equi}, THK) but Table 3 only illustrates the results of the best predictions (size indicators providing the best fit indicated in Table 2). Waldschlager's drag model for fibers (size=diameter in Eq.5) provided the best fit for the observed settling velocity of PES fibers. Figure 4.a compares the observations and estimations from this formulation, showing the good estimation of the magnitude (E=21% and RMSE=1 mm/s, all particles) and the good reproduction of the particle behavior: increase of velocity by biofilm and null effect of fiber length (Figure 4.a.ii). Khatmullina's formulations also provide an adequate estimation of both magnitude and

behavior while Diogualdi's and Dellino's formulations underestimated velocities (higher E in Table 3).

Table 3. Overview of the relative error (E) and root mean square error (RMSE) values of 6 different drag models used to compare and evaluate their performance concerning the different types of MPs used in this study. FW and SW denote experiments performed in fresh- and saltwater, respectively. The model showing the lowest errors for each type of particle is highlighted in bold red font.

Particle	Metric	Case	Waldschlager and Schuttrumpf (2019)	Diogurldi et al (2018)	Khatmullina and Isachenko (2017)	Zhiyao (2008)	Dellino (2005)	This work Dellino+BDI
PES fibers	E (%)	FW-Pristine	**14.87**	63.61	35.54	38.06	63.34	-
		FW-Biofouled	**27.44**	54.58	34.69	40.26	62.57	-
		All	**21.04**	59.17	35.13	39.14	62.96	-
	RMSE (mm/s)	FW-Pristine	**0.62**	1.52	0.99	1.14	1.46	-
		FW-Biofouled	**1.25**	2.09	1.44	1.57	2.37	-
		All	**0.98**	1.82	1.23	1.37	1.96	-
PET sheets	E (%)	SW-Pristine	26.42	**11.00**	-	20.46	**10.68**	**10.68**
		FW-Pristine	23.70	**11.96**	-	20.68	**12.05**	**12.05**
		FW-Biofouled	17.18	**16.32**	-	22.86	21.29	**10.66**
		All	22.43	**13.09**	-	21.33	**14.67**	**11.13**
	RMSE (mm/s)	SW-Pristine	12.97	**5.76**	-	9.89	**5.43**	**5.43**
		FW-Pristine	12.43	**6.55**	-	10.67	**6.70**	**6.70**
		FW-Biofouled	9.44	**9.46**	-	12.88	11.83	**6.75**
		All	11.71	**7.43**	-	11.22	**8.45**	**6.32**
PP sheets	E (%)	FW-Pristine	29.79	25.95	-	25.44	**15.78**	-
		FW-Biofouled	29.17	21.96	-	23.52	**11.85**	-
		All	29.48	23.95	-	24.48	**13.82**	-
	RMSE (mm/s)	FW-Pristine	19.74	15.87	-	16.74	**10.19**	-
		FW-Biofouled	16.98	13.42	-	14.17	**8.01**	-
		All	18.41	14.69	-	15.51	**9.16**	-

All drag models provided good estimations of the magnitude of the settling velocities of PET sheets in both salt and freshwater, particularly Dellino's and Dioguardi's formulations (size=length in Eq. 5) (Table 3), and reproduced the increase of magnitude with particle size, observed for lengths lower than 3.5-4 mm. However, the formulations did not reproduce the decrease of velocity particle with size from 3.5-4 mm length and, as expected, neither the complex effect of biofilm; all the models overestimated the settling velocity of some biofouled particles as they only consider the effect of biofilm on the increase of density. Only Dellino's formulation predicted a slight decrease with size but from 4.5 mm length (see pristine particles in Fig.4.b). According to our results, Dellino's formulation seems to be the best option to predict the settling velocity of sheets (Table 3; pristine particles in Figure 4.b). We took then this

formulation as a base and tried to improve it by incorporating BDI (range 1-3) to take into account the effect of biofilm distribution on the drag coefficient. First, we incorporated BDI so that the original Dellino's formulation is applied for no biofouled particles (BDI=1):

$$C_{D,sheets} = \frac{0.9297}{\Psi^{5.05}\Re_p{}^{0.0799}} BDI^{\alpha} \qquad \text{(Eq. 6)}$$

The Simulated Annealing algorithm[54] was used to find the coefficient α that provides the lowest RMSE between observations and estimations, which was equal to 0.573 (formulation included in Table 2). This formulation implies a decrease by half of the errors for biofouled sheets compared to the original Dellino's formulation (Table 3). Figure 4.b shows a good description of the behavior and magnitude of biofouled sheets with this formulation. The proposed formulation may complete Waldschlager's formulation, which demonstrated an excellent performance for different types of weathered MPs but less suitable predictions for films[52], by adding a new class of drag model for the type of particles "sheets". Nevertheless, our proposed formulation should be further tested and eventually improved with additional experiments that consider sheets of different thicknesses and shapes, including films. Dioguardi's formulation is also a good candidate for estimating the settling velocity of sheets, and particularly handy for incorporation in numerical models as, according to Melkebeke et al.,[26] this formulation provides good settling velocity estimations for MPs of different shapes (fragment, fibers, and films).

All theoretical models provided similar results in the calculation of rising velocities of PP sheets. They provided good estimations of the order of magnitude, but errors were higher than those for settling fibers and sheets (Table 3), particularly for large sizes. The effect of biofilm in decreasing settling velocity was properly described. However, the effect of large sizes in increasing the drag coefficient due to the instabilities in motion was not represented. Figure 4.c compares observations and predictions with Dellino's formulation, which provided the lowest errors (size=length in Eq. 5). A new type of formulation may be needed to predict the behavior

of raising sheets and other types of particles. This will be the aim of future experiments on raising velocity, which should consider different types of non-buoyant MPs, including sheets and films of different shapes, sizes, and polymers.

Further investigation is also needed to take into account the evolution of biofilm over time on settling velocity. Karkanorachaki et al. (2021) proposed empirical formulations of settling velocity increase over time due to biofouling for specific types of polymers, based on sigmoidal curves. However, this type of formulation omits other key physical properties. For example, the present study demonstrated the importance of size on the behavior of sheets. Future researches may aim to integrate the particle size and density as parameters into these velocities – time relationships for different types of aquatic environments.

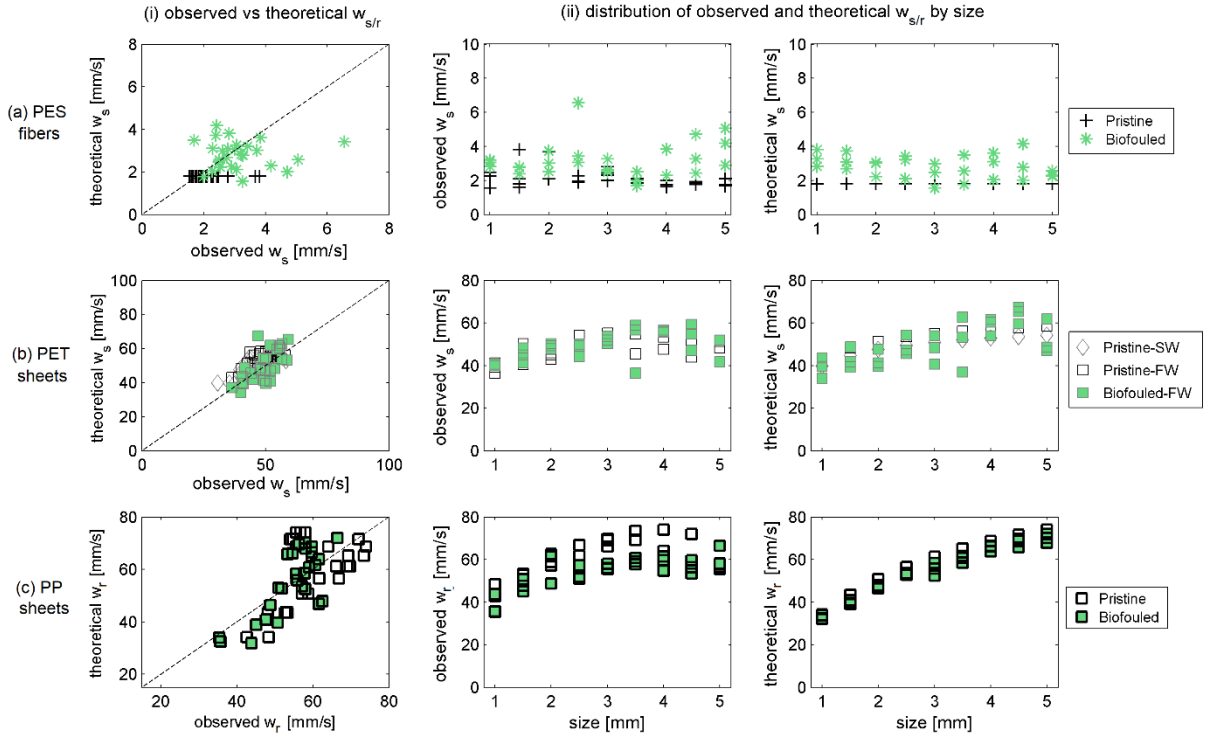

Figure 4. Comparison of observed and theoretical settling (ws) and rising (wr) velocities of pristine and biofouled (a) polyester (PES) fibers, (b) polyethylene terephthalate (PET) sheets, and (c) polypropylene sheets: (i) direct comparison; (ii) distribution

as a function of size. Theoretical velocities were calculated with Waldschläger's formulation for fibers (a), modified-Dellino's formulation (this study) for PET sheets (b), Dellino's formulation for PP sheets (c).

ACKNOWLEDGEMENTS. This work was supported by the French National program EC2CO (Ecosphère Continentale et Côtière) through the project PLASTICBEACH. The weathering of particles was carried out in the context of the project ARPLASTIC funded by Nouvelle Aquitaine Region, AEAG (Agence de l'eau Adour Garonne), SIBA (Syndicat Intercommunal du Bassin d'Arcachon) and the Arcachon Bay Marine Natural Park. We acknowledge the ECOBIOC team from the UMR EPOC for lending us their facilities to carry out the experiments. We also thank Dr. Vincent Marieu for providing the Simulated Annealing algorithm code.

REFERENCES

(1) Cole, M.; Lindeque, P.; Halsband, C.; Galloway, T. S. Microplastics as Contaminants in the Marine Environment: A Review. *Mar. Pollut. Bull.* **2011**, *62* (12), 2588–2597. https://doi.org/10.1016/J.MARPOLBUL.2011.09.025.

(2) Browne, M. A.; Niven, S. J.; Galloway, T. S.; Rowland, S. J.; Thompson, R. C. Microplastic Moves Pollutants and Additives to Worms, Reducing Functions Linked to Health and Biodiversity. *Curr. Biol.* **2013**, *23* (23), 2388–2392. https://doi.org/10.1016/j.cub.2013.10.012.

(3) Cózar, A.; Echevarría, F.; González-Gordillo, J. I.; Irigoien, X.; Úbeda, B.; Hernández-León, S.; Palma, Á. T.; Navarro, S.; García-de-Lomas, J.; Ruiz, A.; Fernández-de-Puelles, M. L.; Duarte, C. M. Plastic Debris in the Open Ocean. *Proc. Natl. Acad. Sci. U. S. A.* **2014**, *111* (28), 10239–10244. https://doi.org/10.1073/PNAS.1314705111/-/DCSUPPLEMENTAL.

(4) Isobe, A.; Uchiyama-Matsumoto, K.; Uchida, K.; Tokai, T. Microplastics in the Southern Ocean. *Mar. Pollut. Bull.* **2017**, *114* (1), 623–626. https://doi.org/10.1016/J.MARPOLBUL.2016.09.037.

(5) Egger, M.; Nijhof, R.; Quiros, L.; Leone, G.; Royer, S.-J.; McWhirter, A. C.; Kantakov, G. A.; Radchenko, V. I.; Pakhomov, E. A.; Hunt, B. P. V; Lebreton, L. A Spatially Variable Scarcity of Floating Microplastics in the Eastern North Pacific Ocean. *Environ. Res. Lett.* **2020**, *15* (11), 114056. https://doi.org/10.1088/1748-9326/abbb4f.

(6) Liu, Y.; Li, Z.; Jalón-Rojas, I.; Wang, X. H.; Fredj, E.; Zhang, D.; Feng, L.; Li, X. Assessing the Potential Risk and Relationship between Microplastics and Phthalates in Surface Seawater of a Heavily Human-Impacted Metropolitan Bay in Northern China. *Ecotoxicol. Environ. Saf.* **2020**, *204*, 111067. https://doi.org/10.1016/J.ECOENV.2020.111067.

(7) de Carvalho, A. R.; Garcia, F.; Riem-Galliano, L.; Tudesque, L.; Albignac, M.; ter Halle, A.; Cucherousset, J. Urbanization and Hydrological Conditions Drive the Spatial and Temporal Variability of Microplastic Pollution in the Garonne River. *Sci. Total Environ.* **2021**, *769*, 144479. https://doi.org/10.1016/J.SCITOTENV.2020.144479.

(8) Lefebvre, C.; Rojas, I. J.; Lasserre, J.; Villette, S.; Lecomte, S.; Cachot, J.; Morin, B. Stranded in the High Tide Line: Spatial and Temporal Variability of Beached Microplastics in a Semi-Enclosed Embayment (Arcachon, France). *Sci. Total Environ.* **2021**, *797*, 149144. https://doi.org/10.1016/J.SCITOTENV.2021.149144.

(9) Dobler, D.; Huck, T.; Maes, C.; Grima, N.; Blanke, B.; Martinez, E.; Ardhuin, F. Large Impact of Stokes Drift on the Fate of Surface Floating Debris in the South Indian Basin. *Mar. Pollut. Bull.* **2019**, *148*, 202–209. https://doi.org/10.1016/J.MARPOLBUL.2019.07.057.

(10) Bermúdez, M.; Vilas, C.; Quintana, R.; González-Fernández, D.; Cózar, A.; Díez-Minguito, M. Unravelling Spatio-Temporal Patterns of Suspended Microplastic Concentration in the Natura 2000 Guadalquivir Estuary (SW Spain): Observations and Model Simulations. *Mar. Pollut. Bull.* **2021**, *170*, 112622. https://doi.org/10.1016/J.MARPOLBUL.2021.112622.

(11) Vega-Moreno, D.; Abaroa-Pérez, B.; Rein-Loring, P. D.; Presas-Navarro, C.; Fraile-Nuez, E.; Machín, F. Distribution and Transport of Microplastics in the Upper 1150 m of the Water

Column at the Eastern North Atlantic Subtropical Gyre, Canary Islands, Spain. *Sci. Total Environ.* **2021**, *788*, 147802. https://doi.org/10.1016/J.SCITOTENV.2021.147802.

(12) Isobe, A.; Kubo, K.; Tamura, Y.; Kako, S.; Nakashima, E.; Fujii, N. Selective Transport of Microplastics and Mesoplastics by Drifting in Coastal Waters. *Mar. Pollut. Bull.* **2014**, *89* (1–2), 324–330. https://doi.org/10.1016/J.MARPOLBUL.2014.09.041.

(13) Chubarenko, I.; Bagaev, A.; Zobkov, M.; Esiukova, E. On Some Physical and Dynamical Properties of Microplastic Particles in Marine Environment. *Mar. Pollut. Bull.* **2016**, *108* (1–2), 105–112. https://doi.org/10.1016/j.marpolbul.2016.04.048.

(14) Hinata, H.; Mori, K.; Ohno, K.; Miyao, Y.; Kataoka, T. An Estimation of the Average Residence Times and Onshore-Offshore Diffusivities of Beached Microplastics Based on the Population Decay of Tagged Meso- and Macrolitter. *Mar. Pollut. Bull.* **2017**, *122* (1–2), 17–26. https://doi.org/10.1016/j.marpolbul.2017.05.012.

(15) Bagaev, A.; Mizyuk, A.; Khatmullina, L.; Isachenko, I.; Chubarenko, I. Anthropogenic Fibres in the Baltic Sea Water Column: Field Data, Laboratory and Numerical Testing of Their Motion. *Sci. Total Environ.* **2017**, *599–600*, 560–571. https://doi.org/10.1016/j.scitotenv.2017.04.185.

(16) Jalón-Rojas, I.; Wang, X. H.; Fredj, E. A 3D Numerical Model to Track Marine Plastic Debris (TrackMPD): Sensitivity of Microplastics Trajectories and Fate to Particle Dynamical Properties and Physical Processes. *Mar. Pollut. Bull.* **2019**, *141*, 256–272.

(17) Defontaine, S.; Sous, D.; Tesan, J.; Monperrus, M.; Lenoble, V.; Lanceleur, L. Microplastics in a Salt-Wedge Estuary: Vertical Structure and Tidal Dynamics. *Mar. Pollut. Bull.* **2020**, *160*, 111688. https://doi.org/10.1016/J.MARPOLBUL.2020.111688.

(18) Díez-Minguito, M.; Bermúdez, M.; Gago, J.; Carretero, O.; Viñas, L. Observations and Idealized Modelling of Microplastic Transport in Estuaries: The Exemplary Case of an

Upwelling System (Ría de Vigo, NW Spain). *Mar. Chem.* **2020**, *222*, 103780. https://doi.org/10.1016/j.marchem.2020.103780.

(19) HALLERMEIER, R. J. Terminal Settling Velocity of Commonly Occurring Sand Grains. *Sedimentology* **1981**, *28* (6), 859–865. https://doi.org/10.1111/J.1365-3091.1981.TB01948.X.

(20) Dietrich, W. E. Settling Velocity of Natural Particles. *Water Resour. Res.* **1982**, *18* (6), 1615–1626. https://doi.org/10.1029/WR018I006P01615.

(21) Ballent, A.; Purser, A.; de Jesus Mendes, P.; Pando, S.; Thomsen, L. Physical Transport Properties of Marine Microplastic Pollution. *Biogeosciences Discuss.* **2012**, *9* (12), 18755–18798. https://doi.org/10.5194/bgd-9-18755-2012.

(22) Kaiser, D.; Kowalski, N.; Waniek, J. J. Effects of Biofouling on the Sinking Behavior of Microplastics. *Environ. Res. Lett.* **2017**, *12* (12). https://doi.org/10.1088/1748-9326/aa8e8b.

(23) Kowalski, N.; Reichardt, A. M.; Waniek, J. J. Sinking Rates of Microplastics and Potential Implications of Their Alteration by Physical, Biological, and Chemical Factors. *Mar. Pollut. Bull.* **2016**, *109* (1), 310–319. https://doi.org/10.1016/J.MARPOLBUL.2016.05.064.

(24) Khatmullina, L.; Isachenko, I. Settling Velocity of Microplastic Particles of Regular Shapes. *Mar. Pollut. Bull.* **2017**, *114* (2), 871–880. https://doi.org/10.1016/j.marpolbul.2016.11.024.

(25) Waldschläger, K.; Schüttrumpf, H. Effects of Particle Properties on the Settling and Rise Velocities of Microplastics in Freshwater under Laboratory Conditions. *Environ. Sci. Technol.* **2019**, *53* (4), 1958–1966. https://doi.org/10.1021/acs.est.8b06794.

(26) Van Melkebeke, M.; Janssen, C.; De Meester, S. Characteristics and Sinking Behavior of Typical Microplastics Including the Potential Effect of Biofouling: Implications for Remediation. *Environ. Sci. Technol.* **2020**, *54* (14), 8668–8680. https://doi.org/10.1021/acs.est.9b07378.

(27) Kooi, M.; Koelmans, A. A. Simplifying Microplastic via Continuous Probability Distributions for Size, Shape,and Density. *Environ. Sci. Technol. Lett.* **2019**, *6* (9), 551–557. https://doi.org/10.1021/ACS.ESTLETT.9B00379/SUPPL_FILE/EZ9B00379_SI_002.XLSX.

(28) Ye, S.; Andrady, A. L. Fouling of Floating Plastic Debris under Biscayne Bay Exposure Conditions. *Mar. Pollut. Bull.* **1991**, *22* (12), 608–613. https://doi.org/10.1016/0025-326X(91)90249-R.

(29) Gewert, B.; Plassmann, M. M.; Macleod, M. Pathways for Degradation of Plastic Polymers Floating in the Marine Environment. *Environ. Sci. Process. Impacts* **2015**, *17* (9), 1513–1521. https://doi.org/10.1039/C5EM00207A.

(30) Jahnke, A.; Arp, H. P. H.; Escher, B. I.; Gewert, B.; Gorokhova, E.; Kühnel, D.; Ogonowski, M.; Potthoff, A.; Rummel, C.; Schmitt-Jansen, M.; Toorman, E.; MacLeod, M. Reducing Uncertainty and Confronting Ignorance about the Possible Impacts of Weathering Plastic in the Marine Environment. *Environ. Sci. Technol. Lett.* **2017**, *4* (3), 85–90. https://doi.org/10.1021/acs.estlett.7b00008.

(31) Wang, J.; Guo, X.; Xue, J. Biofilm-Developed Microplastics As Vectors of Pollutants in Aquatic Environments. *Environ. Sci. Technol.* **2021**, *55* (19), 12780–12790. https://doi.org/10.1021/ACS.EST.1C04466/SUPPL_FILE/ES1C04466_SI_001.PDF.

(32) Lobelle, D.; Kooi, M.; Koelmans, A. A.; Laufkötter, C.; Jongedijk, C. E.; Kehl, C.; van Sebille, E. Global Modeled Sinking Characteristics of Biofouled Microplastic. *J. Geophys. Res. Ocean.* **2021**, *126* (4), e2020JC017098. https://doi.org/10.1029/2020JC017098.

(33) Kooi, M.; Van Nes, E. H.; Scheffer, M.; Koelmans, A. A. Ups and Downs in the Ocean: Effects of Biofouling on Vertical Transport of Microplastics. *Environ. Sci. Technol.* **2017**, *51* (14), 7963–7971. https://doi.org/10.1021/acs.est.6b04702.

(34) Rummel, C. D.; Jahnke, A.; Gorokhova, E.; Kühnel, D.; Schmitt-Jansen, M. Impacts of

554 Biofilm Formation on the Fate and Potential Effects of Microplastic in the Aquatic
555 Environment. *Environ. Sci. Technol. Lett.* **2017**, *4* (7), 258–267.
556 https://doi.org/10.1021/acs.estlett.7b00164.

557 (35) Amaral-Zettler, L. A.; Zettler, E. R.; Mincer, T. J.; Klaassen, M. A.; Gallager, S. M. Biofouling
558 Impacts on Polyethylene Density and Sinking in Coastal Waters: A Macro/Micro Tipping
559 Point? *Water Res.* **2021**, *201*, 117289. https://doi.org/10.1016/J.WATRES.2021.117289.

560 (36) Lobelle, D.; Cunliffe, M. Early Microbial Biofilm Formation on Marine Plastic Debris. *Mar.*
561 *Pollut. Bull.* **2011**, *62* (1), 197–200. https://doi.org/10.1016/j.marpolbul.2010.10.013.

562 (37) Karkanorachaki, K.; Syranidou, E.; Kalogerakis, N. Sinking Characteristics of Microplastics in
563 the Marine Environment. *Sci. Total Environ.* **2021**, *793*, 148526.
564 https://doi.org/10.1016/J.SCITOTENV.2021.148526.

565 (38) Andrady, A. L. Microplastics in the Marine Environment. *Mar. Pollut. Bull.* **2011**, *62* (8),
566 1596–1605. https://doi.org/10.1016/j.marpolbul.2011.05.030.

567 (39) Ross, P. S.; Chastain, S.; Vassilenko, E.; Etemadifar, A.; Zimmermann, S.; Quesnel, S. A.;
568 Eert, J.; Solomon, E.; Patankar, S.; Posacka, A. M.; Williams, B. Pervasive Distribution of
569 Polyester Fibres in the Arctic Ocean Is Driven by Atlantic Inputs. *Nat. Commun. 2021 121*
570 **2021**, *12* (1), 1–9. https://doi.org/10.1038/s41467-020-20347-1.

571 (40) Geyer, R.; Jambeck, J. R.; Law, K. L. Production, Use, and Fate of All Plastics Ever Made. *Sci.*
572 *Adv.* **2017**, *3* (7). https://doi.org/10.1126/SCIADV.1700782/SUPPL_FILE/1700782_SM.PDF.

573 (41) Soulsby, R. L.; Whitehouse, R. J. S. Threshold of Sediment Motion in Coasts and Ports, 1997;
574 In *13th Australiasian Coastal and Engineering Conference and 6th Australasian Port and*
575 *Harbour Conference, Chistchurch, N.Z.*; 1997.

576 (42) Subramanya, K. Fluid Mechanics and Hydraulic Machines : Problems and Solutions. **2011**,
577 633p.

(43) Powers, M. C. A New Roundness Scale for Sedimentary Particles. *J. Sediment. Res.* **1953**, *23* (2), 117–119. https://doi.org/10.1306/D4269567-2B26-11D7-8648000102C1865D.

(44) Dioguardi, F.; Mele, D.; Dellino, P. A New One-Equation Model of Fluid Drag for Irregularly Shaped Particles Valid Over a Wide Range of Reynolds Number. *J. Geophys. Res. Solid Earth* **2018**, *123* (1), 144–156. https://doi.org/10.1002/2017JB014926.

(45) Baba, J.; Komar, P. D. Measurements and Analysis of Settling Velocities of Natural Quartz Sand Grains. *J. Sediment. Petrol.* **1981**, *51* (2), 631–640. https://doi.org/10.2110/JSR.51.631.

(46) Dellino, P.; Mele, D.; Bonasia, R.; Braia, G.; La Volpe, L.; Sulpizio, R. The Analysis of the Influence of Pumice Shape on Its Terminal Velocity. *Geophys. Res. Lett.* **2005**, *32* (21), 1–4. https://doi.org/10.1029/2005GL023954.

(47) Zhiyao, S.; Tingting, W.; Fumin, X.; Ruijie, L. A Simple Formula for Predicting Settling Velocity of Sediment Particles. *Water Sci. Eng.* **2008**, *1* (1), 37–43. https://doi.org/10.1016/S1674-2370(15)30017-X.

(48) Angle, B. R.; Rau, M. J.; Byron, M. L. Effect of Mass Distribution on Falling Cylindrical Particles at Intermediate Reynolds Numbers. *ASME-JSME-KSME 2019 8th Jt. Fluids Eng. Conf. AJKFluids 2019* **2019**, *5*. https://doi.org/10.1115/AJKFLUIDS2019-5458.

(49) Isachenko, I.; Khatmullina, L.; Chubarenko, I.; Stepanova, N. Settling Velocity of Marine Microplastic Particles: Laboratory Tests. *Geophys. Res. Abstr. EGU Gen. Assem.* **2016**, *18*, 2016–6553.

(50) Jianzhong, L.; Xing, S.; Zhenjiang, Y. Effects of the Aspect Ratio on the Sedimentation of a Fiber in Newtonian Fluids. *J. Aerosol Sci.* **2003**, *34* (7), 909–921. https://doi.org/10.1016/S0021-8502(03)00039-9.

(51) Zhong, H.; Lee, C.; Su, Z.; Chen, S.; Zhou, M.; Wu, J. Experimental Investigation of Freely Falling Thin Disks. Part 1. The Flow Structures and Reynolds Number Effects on the Zigzag

Motion. *J. Fluid Mech.* **2013**, *716*, 228–250. https://doi.org/10.1017/JFM.2012.543.

(52) Waldschläger, K.; Born, M.; Cowger, W.; Gray, A.; Schüttrumpf, H. Settling and Rising Velocities of Environmentally Weathered Micro- and Macroplastic Particles. *Environ. Res.* **2020**, *191*, 110192. https://doi.org/10.1016/J.ENVRES.2020.110192.

(53) Fazey, F. M. C.; Ryan, P. G. Biofouling on Buoyant Marine Plastics: An Experimental Study into the Effect of Size on Surface Longevity. *Environ. Pollut.* **2016**, *210*, 354–360. https://doi.org/10.1016/J.ENVPOL.2016.01.026.

(54) Bertsimas, D.; Tsitsiklis, J. Simulated Annealing. *Stat. Sci.* **1993**, *8* (1), 10–15.